BioChip J. (2019) 13(3): 269-276
DOI 10.1007/s13206-019-3302-8

Original Article

Microwell Array-based Digital PCR for Influenza Virus Detection

Christian D. Ahrberg[1,†], Jong Min Lee[1,†] & Bong Geun Chung[1,*]

Received: 18 February, 2019 / Accepted: 16 April, 2019 / Published online: 2 July, 2019

Abstract Digital polymerase chain reaction (dPCR) enables the accurate determination of deoxyribonucleic acid (DNA) copy numbers. In contrast to real-time PCR (qPCR), dPCR can perform quantification without requiring previous standard curve experiments. Furthermore, dPCR is more sensitive for rare targets in genetic samples. Despite the significant advantages of dPCR over qPCR, dPCR is not widely applied yet due to the complicated requirements of instrumentations regarding creating sample subvolumes and the equipment cost associated with this. In this paper, we present a microwell array that can be used for dPCR. The microwell array can be operated with little microfluidic expertise, while it can be manufactured at a unit cost of less than 1$. The amplification results of the microwell array can be analyzed with a custom-written Python script. With this method, we have been able to amplify and quantify complementary deoxyribonucleic acid (cDNA) samples for the H7N9 influenza virus in a concentration range spanning three orders of magnitude (1,000-100,000 copies/μL).

Keywords: Digital PCR, Microwell array, Influenza virus detection, Python image recognition

[1]Department of Mechanical Engineering, Sogang University, 35 Baekbeom-ro, Mapo-gu, Seoul 04107, Republic of Korea
[†]These authors contrilbuted equally.
*Correspondence and requests for materials should be addressed to B. G. Chung (✉bchung@sogang.ac.kr)

Introduction

Polymerase chain reaction (PCR), quantitative PCR (qPCR), and reverse transcription PCR (rtPCR) are valuable tools due to their ability to amplify deoxyribonucleic acid (DNA) and ribonucleic acid (RNA) over several orders of magnitude, followed by subsequent quantification. In contrast to classical PCR approaches the sample volume is divided into several subsamples with volumes in the pico to nanoliter range in digital PCR (dPCR)[1-3]. This is done in such a way that some of the subvolumes contain no copies of the target DNA, while others contain one or more copies. After DNA amplification the number of DNA targets and concentration can be calculated, assuming a Poisson distribution of DNA molecules in the subvolumes[4,5]. Despite the advantages, dPCR experiments using commercial equipment are significantly more expensive than conventional PCR experiments[6]. Furthermore, the microfabrication and microfluidic knowledge required to create subvolumes provides an additional barrier to many users[7].

Three different functions are required for conducting a dPCR experiment: Division of the sample in suitable subsamples, the temperature cycling required for the reaction, and the detection of amplification results in the individual subsamples. For heating of samples, there is a variety of options, which can be easily integrated at low cost. The use of a single heating block, set to a constant temperature, for isothermal amplification is the easiest and most cost effective method[8]. Thin film heaters can also be used, further allowing the following of multistep temperature profiles. These can be fabricated in a reusable[9], or disposable form[10].

In addition, μ-Peltier elements can be used for this task, allowing heating and cooling of samples, with relative simplicity and low costs[11-13]. For detection of PCR amplification results, typically a fluorescent dye is used. While fluorescent probes, like TaqMan-probes, provide specific signals[14] and can be easily used for multiplexed reactions[15], they are relatively expensive. Intercalating fluorescent dyes, like Sybr-Green or EvaGreen for example, provide an unspecific signal with any double stranded DNA at a lower cost per reaction[16]. Commercial digital PCR machines often require a specialized equipment to read the fluorescent signal. The developments in smartphone camera technology and 3D-printing has allowed researchers to create low costs microscope alternatives[17]. Integration of optical filters further allows for fluorescent imaging with sufficient magnification to analyze dPCR experiments[18,19]. A popular method for creating the subsamples required for dPCR is microfluidic droplet technology. This can be done using classical Y-junctions for droplet generation[20], which are typically operated by syringe pumps. Alternatively pressure gradients[21], or centrifugal forces can be used for generating the required droplets[22,23]. On the downside variations in droplet volumes can negatively influence the accuracy of dPCR experiments[24,25]. This effect can be reduced by manufacturing arrays of microwells for partitioning the dPCR sample[26,27]. An example for such an array demonstrated by *K. A. Heyries et al.* consisted of 1,000,000 picoliter-sized microchambers connected by a microchannel[28]. The chambers are filled by flowing the sample through the channel before partitioning the chambers by flushing the channel with an immiscible oil phase. Other designs use three-dimensional (3D) designs with two chambers on top of each other[29]. The bottom chamber contains the microwells, which are open. After filling the bottom chamber with sample, pressure is applied to the top chamber, causing the chamber to swell, partitioning the microwells in the bottom chamber. Other methods use a fractal branching microchannel, connecting microchambers[30]. The poly (dimethylsiloxane) (PDMS)-based device is degassed and the developing negative pressure used to fill the chambers. The partitioning of wells is achieved by the subsequent filling of the channel with an immiscible oil phase. However, these devices often require three dimensional microfabrication and microfluidic knowhow and are thus impractical for typical dPCR users.

Here, we present a PDMS-based microwell array, with a high loading efficiency for the microwells, requiring nothing more than a micropipette. The material costs of PDMS are low, allowing the total material cost for the device shown here to be less than 1$. Thermocycling of the device can be done on a commercial thermocycler usually used for conventional PCR. Fluorescent images of the arrays are taken and results are analyzed using a custom written image recognition algorithm. Following this method, we can perform simple and fast dPCR experiments with little additional equipment requirements compared to qPCR.

Materials and Methods

Microwell Array Fabrication

The PDMS microwell array has been fabricated using a standard soft lithography process as described previously[31,32]. Briefly, photomasks were designed using AutoCAD (Autodesk, USA). Negative photoresist (SU-8 2025, MicroChem Corp, USA) was spin-coated onto 4 inch silicon wafers (Wanxiang Silicon-Peak Electronics Co., China) and the design transferred from the masks by photolithography. Next, PDMS (10:1 monomer:curing agent, Slygard 184, Dow Corning, USA) was spin-coated onto to wafers at 1,200 rpm for 1 minute, resulting in a thickness of 125 μm. After curing of the PDMS at 80 °C for one hour, the individual devices were carefully peeled from the wafer. A microscope cover slide (SPL Life Sciences, Korea) was bound to the back of each device using an oxygen plasma to act as an evaporation barrier. After fabrication devices were inspected by naked eye and bright field microscopy for physical damage, and missing or deformed wells. Devices with visible damage or deformed wells were disposed and not used in further experiments.

dPCR

As a target sequence, synthetic cDNA encoding for haemagglutinin in the H7N9 virus was used for demonstrating the device as previously reported (Supplemental Material Table S1)[33]. The DNA samples for digital PCR experiments were prepared in a solution as follows. To 10 μL of QuandtStudio 3D Digital PCR Master Mix V2 (ThermoFisher, USA) 2.5 μL of EvaGreen Dye (20X in water, Tataa Biocenter, Sweden) and 6 μL bovine serum albumin solution (40 mg/mL in water, Sigma Aldrich, USA) were added. Further 2 μL of a solution containing 10 μM forward and reverse primer was added, resulting in a primer concentration of 500 nM. To this solution cDNA was added and the sample volume adjusted to a total of 20 μL using PCR grade water (Thermo Scientific, USA).

To load the microwells, 5 µL of the PCR solution was pipetted onto the PDMS device, completely covering the area occupied by the wells, which were thus filled by capillary forces[34]. Afterwards, the PDMS device was covered with a microscope objective slide (Marienfeld, Germany), which was treated in an oxygen plasma for 1 minute before. This sealed the device and separated the sample into the microwells. Excess PCR solution, not filled into the microwells was carefully removed from the edges of the device using a paper towel to which it was guided by the channels separating the individual panels of the device. To ensure reliable sealing, the device was then placed in an oven at 80 °C for one minute before being placed on a thermocycler (GeneAmp PCR System 9700, Applied Biosystems, USA). PCR was conducted with the following temperature profile: 10 minutes hot start at 96 °C, followed by 40 cycles of 30 seconds denaturation at 95 °C, 30 seconds annealing at 50 ^{0}C, and 30 seconds extension at 70 °C.

Data Analysis

After thermocycling, devices were placed on a fluorescent microscope (IX37, Olympus, Japan) and images were taken of each panel of the microwell array using a 4X lens (Uplan FLN, Olympus, Japan). For each panel, two images were taken, one with a green filter set for the green fluorescence of the EvaGreen intercalator, and a second with a red fluorescent filter for the ROX reference dye of the master mix. Image sets were then analyzed using a custom-written Python computer program (Supplemental Material S2) utilizing an image recognition technique[35]. In a first step, the program identified the microwell positions in the images of the ROX reference dye using a Hough Transform. Furthermore, the average intensity of all recognized wells was measured by the program in the reference dye images. Next, the green fluorescent images were analyzed; the previously found microwell positions form the ROX reference dye image were transferred to the green fluorescent images and the Python program measured the fluorescence intensity. The measured green fluorescent intensities were normalized using the red fluorescent intensity from the reference wells and normalized well intensities plotted as a histogram. A threshold was defined by determining the maximum of the negative peak and adding the full width half maximum of the negative peak. With this threshold wells were classified as positive (showing amplification) or negative (not showing amplification). Finally, cDNA concentrations were calculated using Poisson statistics (Supplemental Material S3).

Results and Discussion

The microwell array for dPCR consisted of a thin PDMS membrane, containing the microwells and a glass cover to prevent evaporation of sample (Figure 1). Before conducting dPCR experiments, various designs for the PDMS microwell array were tested to optimize loading efficiency and minimize evaporation of sample. Three different well sizes (20, 40, and 80 µm diameter) were tested (Supplemental Figure S1). It was found that while all well sizes showed a high filling efficiency, almost the entire sample evaporated in the larger wells during thermal cycling, visible as significant drops in fluorescence intensity after thermal cycling (Supplemental Figure S2D). Most likely, the larger wells show a higher rate of evaporation, because there is less wall area sealing the PDMS to the bottom glass slide. It could be expected that wells close to the edge of the device would have a higher rate of evaporation, due to the shorter diffusion distance. In experiments however such a relation could not be observed, with all panels displaying a similar evaporation rate (Supplemental Figure S2C). Further experiments were conducted, testing the effect of removing excess solution after filling of the microwells

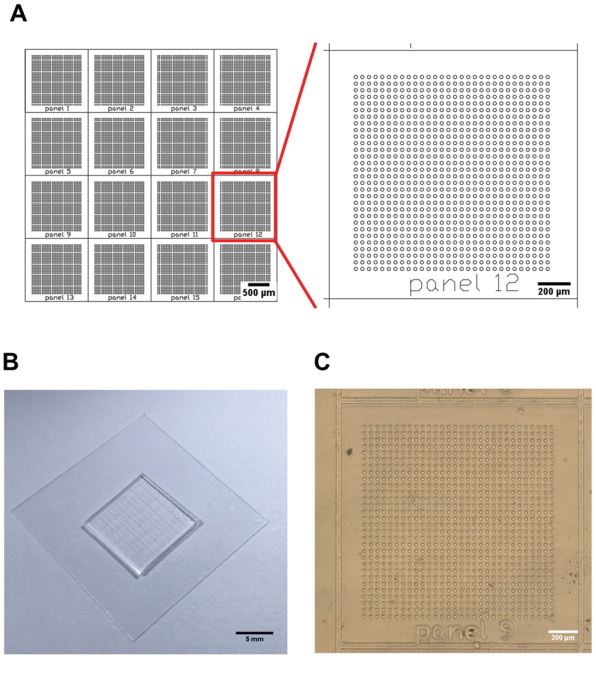

Figure 1. PDMS microwell array for dPCR. CAD drawing of the device consisting out of 16 panels, each containing 30×30 circular microwells with a diameter of 20µm (A). Photograph of the PDMS layer containing the microwells on the glass coverside (B). Bright-field microscope image of an individual panel of the microwell device (C).

by a paper towel. No difference in well filling could be observed when excess solution was removed, thus removal of this does not influence the dPCR results. For further experiments, microwells with a diameter of 20 µm and a pitch of 40 µm were chosen. These wells show a high filling efficiency of more than 99% and low rate of evaporation during thermal cycling (Supplemental Figure S2,3). The device design used for experiments consisted of 16 panels which are all loaded with the same sample at the same time, each containing a 30×30 microwell array. The arrays were separated into panels to allow easier imaging by manual microscopy. In total, the design features 14,400 microwells. Through soft lithography, the diameter of wells was known to be 20 µm with a height of 25 µm, giving a volume of 7.85 pL for each microwell and a total volume of 0.1 µL for all 14,400 microwells. Through the image recognition algorithm utilizing the reference dye for well identification wells with evaporated content were not recognized by the algorithm and thus excluded from analysis. Lastly, it was tested if the wells are deformed during the bonding to the covering glass slide, leading to variations in well volumes. If wells were deformed, they would diverge from the round shape analyzed by the image recognition algorithm, and thus not recognized any more. Comparing the number of identified wells for each panel, to the expected number of wells (Supplemental Figure S2C) it can be seen that all panels show well counts over 98% of the expected number. Thus, there is no significant deformation of the microwells during the binding step. The not recognized wells in most cases could be attributed due to defects, such as missing microwells, in the silicon master used for PDMS microdevice fabrication.

For image analysis, we used an algorithm that identifies well positions using the passive ROX reference dye, measures the green fluorescence of the EvaGreen intercalator for each well, and normalizes the fluorescence value with the reference dye intensity of the according well (Figure 2). The algorithm consisted of four steps for the measurement of fluorescence intensity. First, the Python code opened the images taken with optical filters for the ROX reference dye, and identified well positions in the images using a Hough Transform (Figure 3A-B). Through the use of the Hough transform irregular shaped or microwells obscured by particles could be excluded from analysis. The efficiency and accuracy of the recognition was determined by the two parameters used for the Hough transform, the threshold for the Canny edge detector, and the threshold for detecting the centers of the wells. Further, parameters defining the minimum/ maximum radius of found wells, and the minimum distance between the found wells were used to improve the accuracy. This step required a trade-off between a high

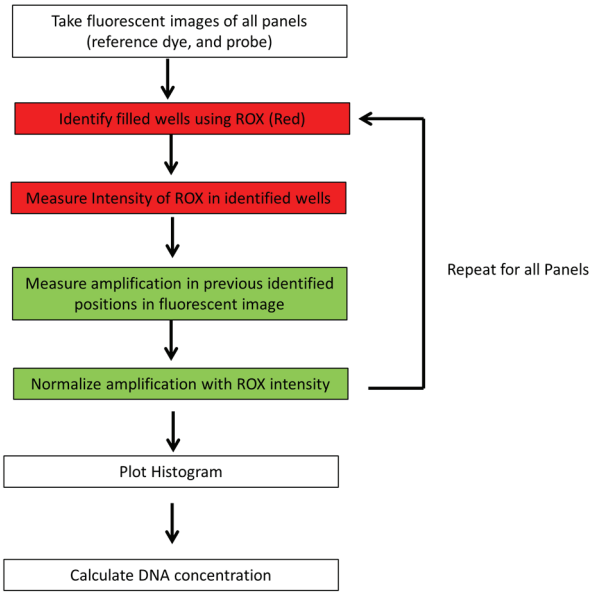

Figure 2. Diagram of the algorithm for the well recognition, fluorescence intensity measurement, and calculation of DNA copy numbers. Steps carried out using the images with an optical filter set for the ROX reference dye are indicated red, and steps carried out using the images with optical filter sets for EvaGreen are indicated in green.

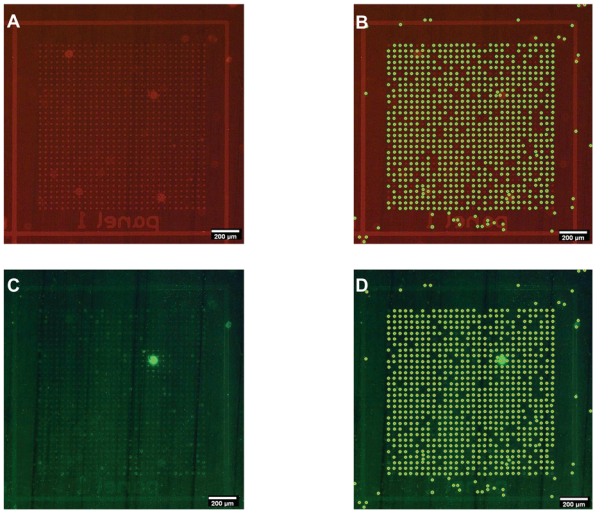

Figure 3. Illustration of the algorithm of the Python program. Fluorescence image taken of one panel using optical filters for the ROX reference dye (A), microwells recognized in the ROX image using a Hough transform image recognition method (B). Fluorescence image taken of the same panel using optical filters for the EvaGreen intercalating dye (C), and microwells identified from the ROX image as transferred to EvaGreen image (D).

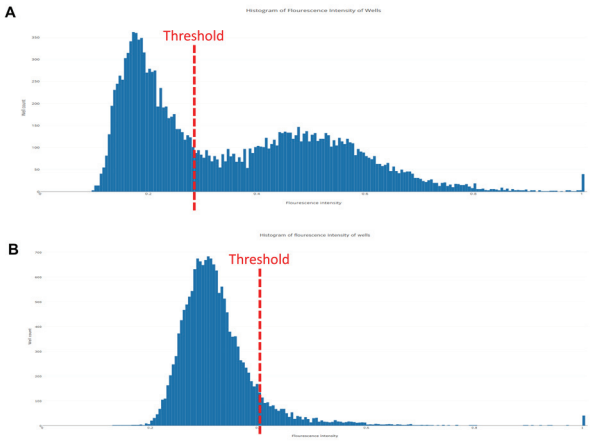

Figure 4. Two examples of Histograms of normalized, average fluorescence intensity for an experiment with a cDNA concentration of 100,000 copies/µL (A), and a second experiment with a cDNA concentration of 10,000 copies/µL (B).

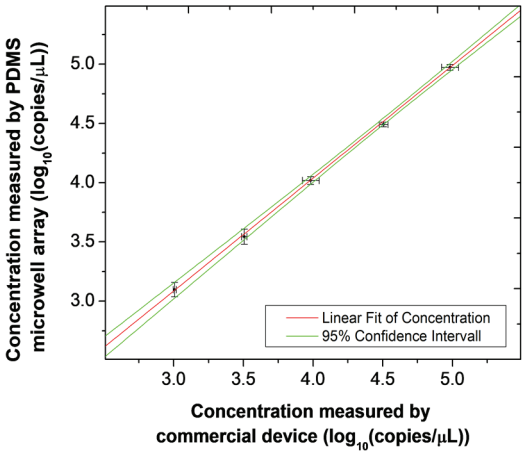

Figure 5. Graph of cDNA concentration as measured by a commercial dPCR device against the concentrations measured by microwell array and algorithm. A linear curve was fitted to the data (red), the upper confidence level (UCL) and lower confidence level (LCL) are denoted in green. The slope of the fitted linear function is 0.95±0.02.

recognition rate of wells, which also lead to a high number of false well recognitions, and a low recognition rate of wells with a low number of false well recognitions. In the next step, the algorithm accessed the images taken with the optical filter set for the green fluorescing EvaGreen intercalator. The average fluorescence intensity was measured in the wells previously identified from the ROX reference dye images (Figure 3C-D). Before plotting the average well fluorescence intensity as a histogram, well intensities were normalized with the average intensity of the ROX dye of the corresponding wells (Figure 4). Through the normalization, we compensate for two different effects. On the one side, this removes artefacts originating from different illumination intensities, which can originate through the light source or through artefacts form the spin-coating process. On the other side, this removes effects of uneven well filling from the histogram. It was found that the simple normalization of fluorescence intensity increased the signal to noise ratio, visible in the bimodal distribution in the histograms becoming more identifiable (Supplemental Figure S4).

The threshold for separating positive from negative wells was defined by adding the full width half maximum to the average fluorescence intensity of the peak with the negative wells. Assuming that the peaks are following normal a distribution, this would correspond to about 2.5 standard deviations. This method created a population of positive and a population of negative wells with no rain in the middle. For our method two assumptions have to be made: (1) the peak with the lower concentration corresponds to negative wells, and (2) the peak for the negative wells is symmetric. The symmetry of the negative peak was confirmed by a control experiment with no DNA template (Supplemental Figure S5C). When a sample with a very high DNA concentration is tested it could be the case that there is only a positive peak present, which would lead to a false result with our method. However, in this case it can be easily seen by eye from the fluorescent microscope images that all wells are positive (Supplemental Figure S5B/E). In this case, the experiment should be repeated with a diluted sample.

In dPCR experiments with cDNA concentrations spanning three orders of magnitude (10^3-10^5 copies/µL in the dPCR mix), it was found that the microarray presented here gave an accurate measurement of the concentrations (Figure 5). All measurements were repeated in three independent experiments, with only small variations between the measurements (Supplemental Figure S6). From these measurements and the comparison to the commercial device, a precision of 7.5% was determined for the PDMS microwell array combined with the analysis algorithm. The DNA concentrations measured by the PDMS microwell array were identical to measurements of the same sample with a commercial dPCR device. For the measurements of the commercial device the included software was used for results analysis including automated setting of thresholds. As the measurements by our PDMS microwell array are identical to the ones of the commercial device, this indicates the suitability of our method of setting the threshold. This further indicates that the wells are tightly sealed and there is no cross-

talk between wells, as crosstalk would lead to an overestimation of the DNA concentration by generating false positives. In theory, the upper limit of detection of our device is about 6×10^5 copies/μL in the dPCR mix, assuming 99% of all wells to be positive, with all wells being filled and no experimental noise (Supplemental Material S4). However, considering experimental factors and imperfect well filling a more realistic upper limit of detection can be considered at 3×10^5 copies/μL in the dPCR mix (Supplemental Figure S5). This limit could be increased by decreasing the well size. For example, if the volume of the microwells is reduced by a factor of 2, this would lead to an increase in the upper detection limit by a factor of 2. For the lower limit of detection, one would expect to be able to detect a single copy of DNA in the entire microwell array. Considering the stochasticity of DNA distribution in the wells, this would require a theoretical concentration of more than 10 copies/μL, so that one device has a 95% chance of containing at least one copy of DNA. In practice, however, a number of noise sources, such as dark fluorescence from the intercalating dye, dust particles in the PDMS, or other fluorescent materials, lead to false signals. Thus, as looking at the dark count from a negative control, the lower limit of detection of our system is 700 copies/ μL (Supplemental Figure S5A-C). For comparison, the detection range of the commercial device, as recommended by the manufacturer, is from 860 to 2,300 copies/μL. The limit of quantification, which we define as the baseline signal plus 5 standard deviations would thus be 1000 copies/μL (Supplemental Figure S5A-C). The lower limit of detection could be improved by using a different reporter, such as TaqMan probes, eliminating some of the noise coming from the reporter dye. As PDMS is a commonly used material for PCR the reagents and dye could be exchanged easily[21,28-30]. Further exchanging the PDMS against another material, less prone to collecting dust and other contaminations, could lead to further improvement. Overall, the detection range and limits of detection are comparable to other recently presented devices[30], while our device is simpler to fabricate and operate by untrained users.

Conclusions

Here, we developed a microwell array-based dPCR for detection of influenza virus. The device can be fabricated using conventional soft lithography techniques and conventional thermocyclers can be used for the PCR. Analysis of amplification results and quantification of target DNA was performed using fluorescent microscopy and a custom-written image analysis program. If a TaqMan dye would be used, the limit of detection could be reduced. Furthermore, the combination of a TaqMan probe and intercalating dye would allow for the detection of multiple amplicons at the same time in a near future. Further the fluorescent microscope used for detection could be replaced by a smartphone camera modified with corresponding optical filters. This would make this device a viable approach for dPCR in portable or cost sensitive applications.

Acknowledgements This research was supported by BioNano Health-Guard Research Center funded by the Ministry of Science and ICT (MSIT) of Korea as Global Frontier Project (Grant number H-GUARD_ 2013M3A6B2078950 (2014M3A6B2060302)). This work was also supported by the National Research Foundation (NRF) of Korea grant funded by the MSIT (Grant number 2017R1C1B3012221, 2017H1D3A1A 02013996).

Conflict of Interests The authors declare no competing financial interests.

References

1. Sykes, P. J., Neoh, S. H., Brisco, M. J., Hughes, E., Condon, J. & Morley, A. A. Quantitation of targets for PCR by use of limiting dilution. *BioTechniques* **13**, 444-449, (1992).
2. Vogelstein, B. & Kinzler, K. W. Digital PCR. *Proc. Natl. Acad. Sci. U. S. A.* **96**, 9236-9241, (1999).
3. Nagamune, T. Biomolecular engineering for nanobio/ bionanotechnology. *Nano Convergence* **4**, 9, (2017).
4. Rödiger, S., Burdukiewicz, M., Blagodatskikh, K., Jahn, M. & Schierack, P. R as an Environment for Reproducible Analysis of DNA Amplification Experiments. *The R Journal* **7**, 127-150, (2015).
5. Dorazio, R. M. & Hunter, M. E. Statistical Models for the Analysis and Design of Digital Polymerase Chain Reaction (dPCR) Experiments. *Anal. Chem.* **87**, 10886-10893, (2015).
6. Whale, A. S., Huggett, J. F., Cowen, S., Speirs, V., Shaw, J., Ellison, S., Foy, C. A. & Scott, D. J. Comparison of microfluidic digital PCR and conventional quantitative PCR for measuring copy number variation. *Nucleic Acids Res.* **40**, e82, (2012).

7. Wang, Y., Southard, K. M. & Zeng, Y. Digital PCR using micropatterned superporous absorbent array chips. *Analyst* **141**, 3821-3831, (2016).
8. Liu, Q., Zhang, X., Chen, L., Yao, Y., Ke, S., Zhao, W., Yang, Z. & Sui, G. A sample-to-answer labdisc platform integrated novel membrane-resistance valves for detection of highly pathogenic avian influenza viruses. *Sens. Actuators B* **270**, 371-381, (2018).
9. Ahrberg, C. D. & Manz, A. Superheated droplets for protein thermal stability analyses of GFP, BSA and Taq-polymerase. *RSC Adv.* **6**, 42076-42080, (2016).
10. Costantini, F., Petrucci, G., Lovecchio, N., Nardecchia, M., Nascetti, A., Cesare, G. d., Tedeschi, L., Domenici, C., Ruggi, A., Placidi, P., Scorzoni, A. & Caputo, D. Integrated Sensor System for DNA Amplification and Separation Based on Thin Film Technology. *IEEE Trans. Compon. Packag. Manuf. Technol.* 8, 1141-1148, (2018).
11. George, M., Gomex, A., Zhong, J., Gomez, F.A. & Scherer, A. Microfluidic polymerase chain reaction. *Appl. Phys. Lett.* **93**, 243901, (2008).
12. Maltezos, G., Johnston, M. & Scherer, A. Thermal management in microfluidics using micro-Peltier junctions. *Appl. Phys. Lett.* **87**, 154105, (2005).
13. Pardy, T., Rang, T. & Tulp, I. Thermal Analysis of a Disposable, Instrument-Free DNA Amplification Lab-on-a-Chip Platform. *Sensors* **18**, (2018).
14. Giulietti, A., Overbergh, L., Valckx, D., Decallonne, B., Bouillon, R. & Mathieu, C. An Overview of Real-Time Quantitative PCR: Applications to Quantify Cytokine Gene Expression. *Methods* **25**, 386-401, (2001).
15. Zhong, Q., Bhattacharya, S., Kotsopoulos, S., Olson, J., Taly, V., Griffiths, A.D., Link, D.R. & Larson, J. W. Multiplex digital PCR: breaking the one target per color barrier of quantitative PCR. *Lab Chip* **11**, 2167-2174, (2011).
16. Ahrberg, C. D. & Neužil, P. Doubling Throughput of a Real-Time PCR. *Sci. Rep.* **5**, 12595, (2015).
17. Chiong, H. S., Fang, J. L. L. & Wilson, G. Telemanufactured affordable smartphone anterior segment microscope. *Clin. Exp. Optom.* **99**, 580-582, (2016).
18. Selck, D. A., Karymov, M. A., Sun, B. & Ismagilov, R. F. Increased Robustness of Single-Molecule Counting with Microfluidics, Digital Isothermal Amplification, and a Mobile Phone versus Real-Time Kinetic Measurements. *Anal. Chem.* **85**, 11129-11136, (2013).
19. Kim, J.-H., Joo, H.-G., Kim, T.-H. & Ju, Y.-G. A smartphone-based fluorescence microscope utilizing an external phone camera lens module. *BioChip J.* **9**, 285-292, (2015).
20. Schaerli, Y., Wootton, R. C., Robinson, T., Stein, V., Dunsby, C., Neil, M. A. A., French, P. M. W., deMello, A. J., Abell, C. & Hollfelder, F. Continuous-Flow Polymerase Chain Reaction of Single-Copy DNA in Microfluidic Microdroplets. *Anal. Chem.* **81**, 302-306, (2009).
21. Tanaka, H., Yamamoto, S., Nakamura, A., Nakashoji, Y., Okura, N., Nakamoto, N., Tsukagoshi, K. & Hashimoto, M. Hands-Off Preparation of Monodisperse Emulsion Droplets Using a Poly (dimethylsiloxane) Microfluidic Chip for Droplet Digital PCR. *Anal. Chem.* **87**, 4134-4143, (2015).
22. Schuler, F., Schwemmer, F., Trotter, M., Wadle, S., Zengerle, R., von Stetten, F. & Paust, N. Centrifugal step emulsification applied for absolute quantification of nucleic acids by digital droplet RPA. *Lab Chip* **15**, 2759-2766, (2015).
23. Schuler, F., Trotter, M., Geltman, M., Schwemmer, F., Wadle, S., Dominguez-Garrido, E., López, M., Cervera-Acedo, C., Santibanez, P., von Stetten, F., Zengerle, R. & Paust, N. Digital droplet PCR on disk. *Lab Chip* **16**, 208-216, (2016).
24. Jacobs, B. K. M., Goetghebeur, E. & Clement, L. Impact of variance components on reliability of absolute quantification using digital PCR. *BMC Bioinf.* **15**, 283 (2014).
25. Huggett, J. F., Cowen, S. & Foy, C. A. Considerations for Digital PCR as an Accurate Molecular Diagnostic Tool. *Clin. Chem.* **61**, 79-88, (2015).
26. Bhat, S., Herrmann, J., Armishaw, P., Corbisier, P. & Emslie, K. R. Single molecule detection in nanofluidic digital array enables accurate measurement of DNA copy number. *Anal. Bioanal. Chem.* **394**, 457-467, (2009).
27. Seo, Y.T., Jeong, S., Lee, J.K., Choi, H.S., Kim, J. & Lee, H.Y. Innovations in biomedical nanoengineering: nanowell array biosensor. *Nano Convergence* **5**, 9, (2018).
28. Heyries, K. A., Tropini, C., VanInsberghe, M., Doolin, C., Petriv, O. I., Singhal, A., Leung, K., Hughesman, C. B. & Hansen, C. L. Megapixel digital PCR. *Nat. Methods.* **8**, 649-651, (2011).
29. Men, Y., Fu, Y., Chen, Z., Sims, P. A., Greenleaf, W. J. & Huang, Y. Digital Polymerase Chain Reaction in an Array of Femtoliter Polydimethylsiloxane Microreactors. *Anal. Chem.* **84**, 4262-4266, (2012).
30. Zhu, Q., Xu, Y., Qiu, L., Ma, C., Yu, B., Song, Q., Jin, W., Jin, Q., Liu, J. & Mu, Y. A scalable self-priming fractal branching microchannel net chip for digital PCR. *Lab Chip* **17**, 1655-1665, (2017).
31. Ha, J. H., Kim, T. H., Lee, J. M., Ahrberg, C. D. & Chung, B. G. Analysis of 3D multi-layer microflui-

dic gradient generator. *Electrophoresis* **38**, 270-277, (2017).
32. Choi, J. W., Lee, J. M., Kim, T. H., Ha, J. H., Ahrberg, C. D. & Chung, B. G. Dual-nozzle microfluidic droplet generator. *Nano Convergence* **5**, 12, (2018).
33. Ahrberg, C. D., Manz, A. & Neuzil, P. Single Fluorescence Channel-based Multiplex Detection of Avian Influenza Virus by Quantitative PCR with Intercalating Dye. *Sci. Rep.* **5**, 11479, (2015).
34. Rondelez, Y., Tresset, G., Tabata, K. V., Arata, H., Fujita, H., Takeuchi, S. & Noji, H. Microfabricated arrays of femtoliter chambers allow single molecule enzymology. *Nat. Biotechnol.* **23**, 361, (2005).
35. Ahrberg, C. D., Lee, J. M. & Chung, B. G. Poisson statistics-mediated particle/cell counting in microwell arrays. *Sci. Rep.* **8**, 2438, (2018).